Electrochimica Acta 63 (2012) 251–255

Contents lists available at SciVerse ScienceDirect

Electrochimica Acta

journal homepage: www.elsevier.com/locate/electacta

Fabrication of Pt nano-dot-patterned electrode using atomic force microscope-based indentation method

Minoru Umeda*, Akira Kishi, Sayoko Shironita

Department of Materials Science and Technology, Faculty of Engineering, Nagaoka University of Technology, 1603-1, Kamitomioka, Nagaoka, Niigata 940-2188, Japan

ARTICLE INFO

Article history:
Received 9 August 2011
Received in revised form
22 December 2011
Accepted 22 December 2011
Available online 30 December 2011

Keywords:
Nano-dot pattern fabrication
Pt electrodeposition
Glassy carbon electrode
Nano indentation
Polymer overcoat layer

ABSTRACT

We developed a new technique for fabricating an electrocatalytic surface of defined morphology in which the particle size and interparticle distance are controlled independently on an electroconductive substrate. Firstly, an electroconductive glassy carbon substrate was overcoated by a uniform insulating polymer layer as a mask. Secondly, the polymer coated substrate was indented in nano size using an atomic force microscope (AFM) cantilever to expose the carbon surface. Thirdly, Pt particles were electrodeposited only on the exposed area of the glassy carbon. To expose a small area of the glassy carbon, a 10 ± 1-nm thick insulating polymer overcoat layer was prepared, and a cantilever indentation was performed at an optimized loading force of 3.6 μN. The smallest exposed area obtained was 20 nm × 40 nm. Thereafter, Pt electrodeposition was conducted at an electrode potential of 0.12 V vs RHE so that the Pt particles could be located only at the exposed deposition sites. Thus, Pt deposition of 30–60 nm in diameter was successfully achieved at an arbitrary proportion of the interparticle distance.

1. Introduction

Electrocatalysts comprised of nano-sized and zero-dimension particles on an electroconductive support are widely utilized in practical applications in fuel cells [1], electrolyzers [2], and electrochemical sensors [3–5], due to their high effective surface area. Almost all of the electrocatalysts have a two-component structure in which nano-sized catalytic particles are loaded on an electroconductive support. To functionalize the electrocatalytic activity, the particle size and interparticle distance are believed to play an important role in the electrocatalysts [6–8]. A smaller particle size yields a larger surface area, which will provide a larger number of reaction sites. However, there is no research report in the field of electrocatalysts in which particle size and interparticle distance are independently controlled. With regard to the field of electrocatalysts, it is worthwhile to clarify the relationship between particle size and interparticle distance.

To realize a well-characterized electrocatalyst model in which the particle size and interparticle distance are controlled independently, a metallic nano fabrication on an electroconductive substrate seems to be an effective approach [9,10]. There are two metal nano fabrication techniques: Maskless fabrication [11–21] and mask fabrication [22–39]. Maskless fabrication uses a dip pen [11–13], microcontact printing [14,15], metal deposition onto a sample using a charged surface potential [16–20], and an indent method [21]. For mask fabrication, part of the mask prepared on a substrate is removed in certain areas by an electron beam [22–24], ion-beam [25–27], chemical etching [28–30], an atomic force microscope (AFM) cantilever [31–34], mold [35–39], etc., where the metallic areas are selectively deposited on the substrate in places where the mask was removed.

However, thus far, metallic nano fabrication studies have focused on electrode-pattern formation for semiconductor devices [13,15,17,19,20,22–25,28,30–36,39]. Therefore, the metallic nano fabrication has used a technique that deposits a single-dimension line of metal on a semiconductor Si substrate, but there are no research reports on the deposition of zero-dimensional metal dots on an electroconductive substrate.

To fabricate the electrocatalytic surface of defined morphology, our attention was focused on a mask fabrication method that deposits metallic nano particles on the substrate. Previously, we developed a nano peel-off fabrication technique for Pt electrodeposition, in which an insulating polymer overcoat layer was first prepared on an electroconductive glassy carbon substrate, and then the polymer overcoat layer was peeled off by a scratch technique using an AFM cantilever. Consequently, Pt deposition of 100–150 nm in diameter was successfully achieved by adjusting the interparticle distance [40].

* Corresponding author. Tel.: +81 258 47 9323; fax: +81 258 47 9323.
E-mail address: mumeda@vos.nagaokaut.ac.jp (M. Umeda).

0013-4686/$ – see front matter © 2011 Elsevier Ltd. All rights reserved.
doi:10.1016/j.electacta.2011.12.096

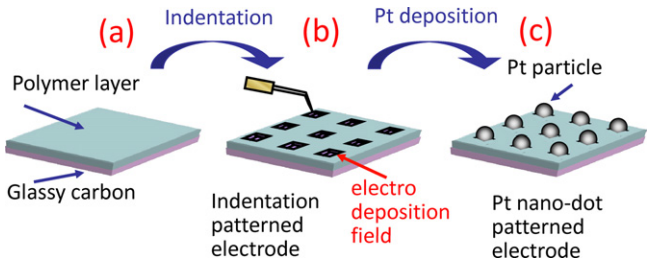

Fig. 1. Schematic illustration of the Pt nano-dot patterning process: (a) a thin polymer insulating layer is overcoated on glassy carbon; (b) nano indentation of the overcoat layer using a cantilever of AFM; and (c) Pt electrodeposition.

In the present work, the mask fabrication method will be further improved, because the previously prepared 100–150 nm Pt is much larger than that used for the electrocatalysts. Because the Pt deposition size is proportional to the exposed electrode area, we will utilize the mask fabrication method by employing a nano-indentation technique. Firstly, a thin insulating polymer overcoat layer was prepared on an electroconductive glassy carbon substrate. Secondly, a small part of the polymer overcoat layer is removed by an indentation with the AFM cantilever. In this process, the exposed electrode area and interexposed distance of the polymer overcoat layer are controlled by changing the indentation force of the cantilever and the interindentation distance. Pt particles are then electrodeposited only on the exposed area of the glassy carbon. Using this procedure, the Pt electrocatalyst of defined morphology which has much smaller Pt particles is fabricated successfully.

2. Experimental

2.1. Preparation of glassy carbon with polymer overcoat

A glassy carbon plate was purchased from Tokai Carbon Co., Ltd. (GC-20SS). The glassy carbon plate was cut into 1 cm^2 pieces. One side of the glassy carbon plate was polished using a buff (Refinetec Co., Ltd., No. 55-308) with an alumina suspension (Union Carbide, 0.05 μm in diameter). Thereafter, the polished glassy carbon was rinsed using Milli-Q water and then dried. The roughness of the polished surface was measured using an AFM (Shimadzu, SPM-9500 J3), and the arithmetic average roughness (R_a) was around 2.2 nm.

Next, the polished glassy carbon was immersed in a perfluorinated resin solution (Asahi Glass Co., Ltd, Cytop, CTX-109, 1–2 wt.%), and it was removed at a constant speed of 180 μm s^{-1} using a motorized micromanipulator (Narishige Co., Ltd., MM-80). After this dip-coating procedure, the glassy carbon was dried at 80 °C in an oven chamber for 1 h to form a 10–22-nm thick polymer overcoat layer.

2.2. Nanoindentation of the polymer overcoat

Nano indentation of the polymer overcoat layer was conducted using an AFM equipped with a Si cantilever (Nano World, PPP-NCHR) to expose the glassy carbon surface. The curvature radius of the used Si-cantilever tip was smaller than 10 nm so that the aspect ratio of the prepared indentation pinhole could be high. The loading force of the cantilever was 0.9–4.3 μN. After the indentation, the sample was immersed for 5 min in Milli-Q water to remove the polymer debris by ultrasonic cleaning.

2.3. Pt electrodeposition on the nano-indented substrate

The nano-indentation sample was used as a working electrode for Pt electrodeposition. Ag/Ag_2SO_4 [41], and Pt wire was used for both the reference and counter electrodes. Using a potentiostat (ALS, Model 802B), Pt electrodeposition was carried out in a solution mixture of 5 mmol dm^{-3} $H_2Pt(OH)_6$ + 3.0 mol dm^{-3} H_2SO_4 for 3 s at a stationary electrode potential of −0.65 to −0.45 V vs Ag/Ag_2SO_4 (0.1–0.3 V vs RHE)at 20 °C. Here, $H_2Pt(OH)_6$ was used for a stable Pt deposition. The sample was then thoroughly rinsed in Milli-Q water and dried.

The sample surface was characterized by AFM and a scanning electronmicroscope (SEM) (JEOL, JSM-6060A) coupled with energy dispersive X-ray spectroscopy (EDS) (JEOL, JED-2300).

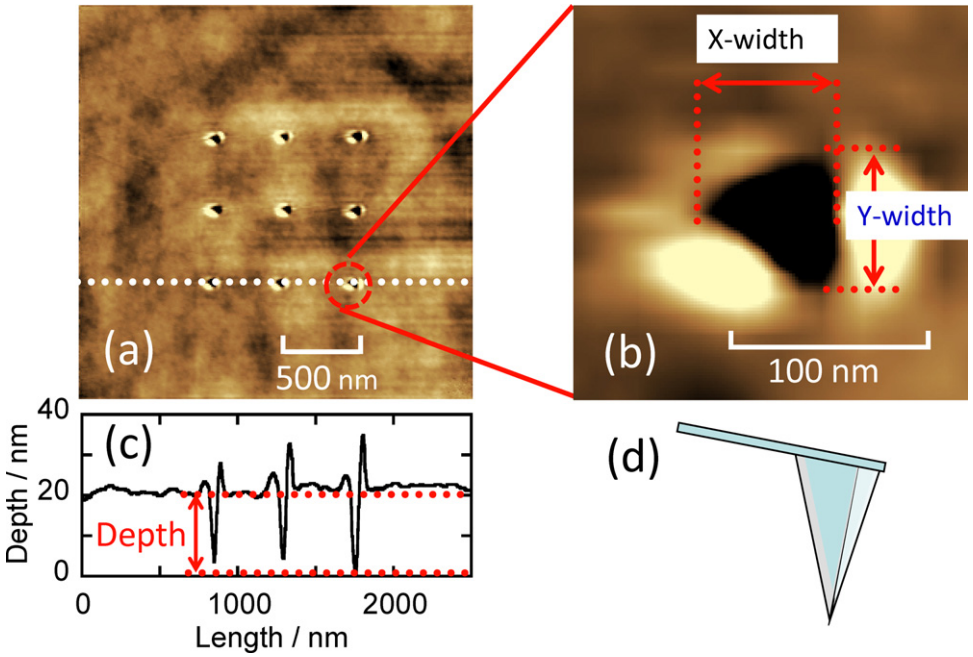

Fig. 2. (a) AFM topography of a glassy carbon substrate with a polymer overcoat layer of 21 ± 1 nm thick after the cantilever indentation at 0.9 μN loading force. (b) A magnification of the indented spot. (c) Cross-sectional profile of the dashed line of (a). (d) Illustration of the cantilever tip.

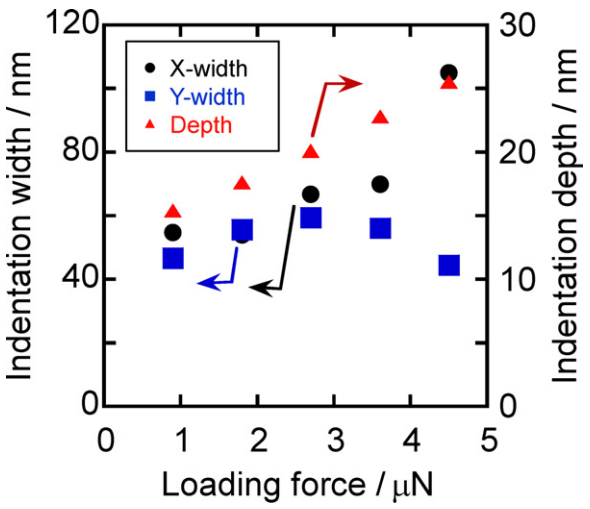

Fig. 3. Cantilever loading force dependence of the indentation depth and indentation widths for the 21 ± 1-nm polymer-coated glassy carbon. The X- and Y-widths are defined in Fig. 2(b).

3. Results and discussion

3.1. Relationship between indentation force and indentation widths

Previously, we employed the mask-scratch technique which was developed to peel-off the polymer overcoat layer by scanning the AFM cantilever in the X and Y directions. The cantilever operating area of 80 nm × 80 nm and the following electrodeposition resulted in Pt particles of 100–150 nm in diameter [40]. To diminish the peel-off area, the mask-scratch technique has been improved with a mask-indentation technique in the present study. This is a new technique in which an AFM cantilever indentation on the polymer-coated electrode creates a small pinhole for the Pt electrodeposition.

According to the concept shown in Fig. 1, nano indentations were performed on a 21 ± 1-nm thick insulating layer formed on the glassy carbon at a cantilever loading force of 0.9 μN. Fig. 2(a) shows the surface topography of the resulting sample measured by an AFM, in which nine indented pinholes prepared at an interindentation distance of 500 nm are seen. Fig. 2(b) demonstrates a magnification of one pinhole. The triangular dark spot reflects the shape of the indented cantilever as illustrated in the figure. Fig. 2(c) represents a cross-sectional view of the dotted line of Fig. 2(a). The cross-sectional profile points out that the depth of the indented pinhole is less than the thickness of the polymer layer. Therefore, a part of polymer layer still remains and prevents the following electrodeposition.

Next, the influence of the loading force to the indentation shape was investigated. As is demonstrated in Fig. 2(b), the indentation shape can be defined by the X- and Y-widths. Fig. 3 shows the relationships between the loading force and the indentation widths and also between the loading force and the indentation depth. It can be seen in the figure that the X-width and the indentation depth increase according to an increase in the loading force. The indentation depth becomes equal to the polymer thickness at 2.7 μN loading force and exceeds that at a loading force of larger than 3.6 μN. However, the Y-width increases up to the 2.7 μN loading force and then decreases. This strongly suggests that the tip of the cantilever was damaged. It is therefore considered that a loading force of 2.7–3.6 μN is appropriate to create the indentation for the Pt electrodeposition.

3.2. Pt electrodeposition at the mask-indentation electrode

First, Pt electrodeposition was performed for the 2.7 μN-indentation sample. However, no Pt deposition occurred. This result can be explained by a residual portion of the insulating polymer at the bottom of the pinhole. Accordingly, an exposure of the glassy carbon to an electrolytic solution will be needed for the Pt deposition.

Next, by employing the 3.6-μN indentation sample, another Pt electrodeposition was attempted. Fig. 4(a) shows the surface profile of the sample before Pt deposition. Nine indentation spots

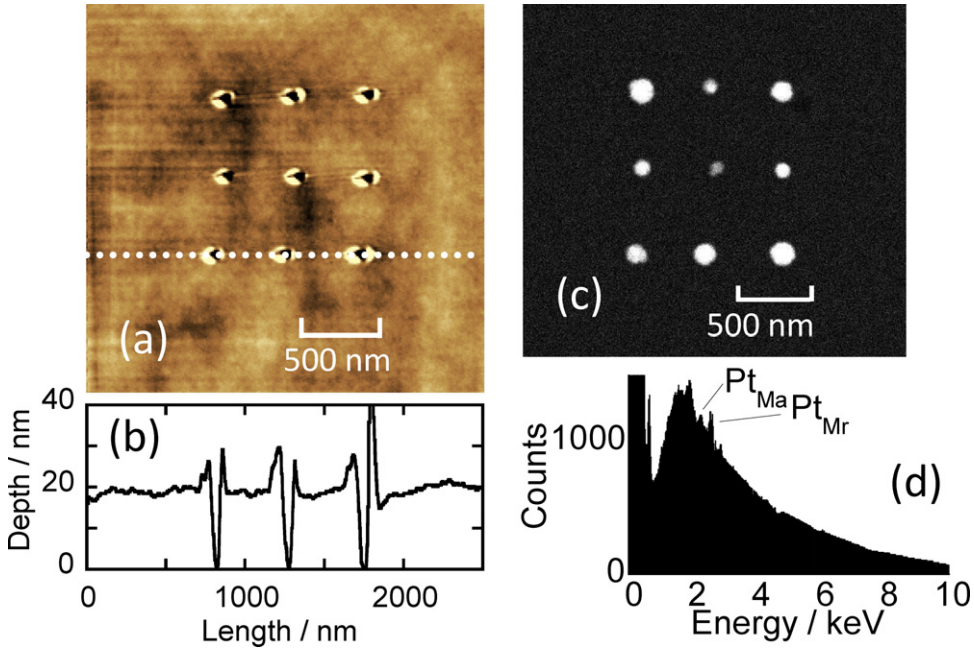

Fig. 4. (a) AFM image of a glassy carbon substrate coated with a 21 ± 1 nm polymer layer using the cantilever indentation at 3.6 μN loading force. (b) Cross-sectional profile of the dashed line of (a). (c) SEM image after the Pt electrodeposition on the same sample. (d) EDS analysis of the top-right particle of (c).

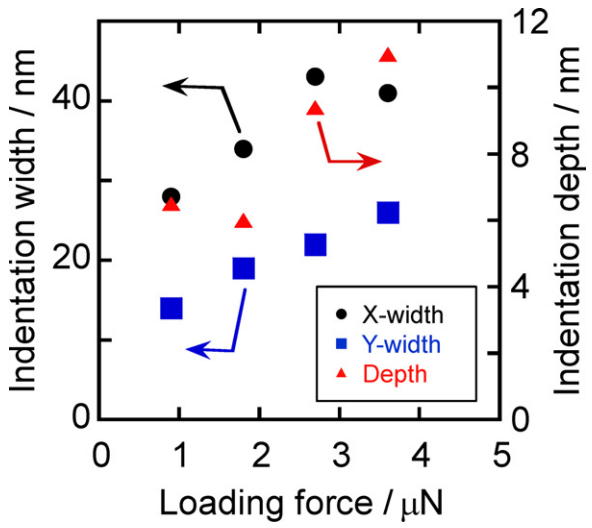

Fig. 5. Cantilever loading force dependence of the indentation depth and indentation widths for the 10 ± 1-nm polymer-coated glassy carbon. The X- and Y-widths are defined in Fig. 2(b).

of 70 nm × 50 nm width and a 500-nm interdistance are seen. A cross-sectional profile of the dotted line demonstrated in Fig. 4(b) reveals that the depths of the indentations are larger than the polymer thickness. This ensures the exposure of the glassy carbon.

Fig. 4(c) shows an SEM image after Pt electrodeposition at 0.1 V vs RHE on the sample in Fig. 4(a). In the figure, nine single particles of 60–140 nm in diameter can be recognized. The result of SEM-EDS analysis of the top-right particle is shown in Fig. 4(d). This ensures that the Pt deposition certainly occurred only at the indentation spots.

However, when we compare Fig. 4(a) and (c), the Pt particle size is known to be larger than that of the indentation spots. This is because that the Pt deposition progresses in the X- and Y-directions on the surface of polymer after the indented pinhole was filled by the deposited Pt.

3.3. Downsizing of deposited Pt using thinner-mask indentation

An effective way to downsize the Pt deposition is to use a thinner polymer layer coated on the glassy carbon, because the indentation width can be decreased. A further thinner polymer layer of 10 ± 1 nm was then prepared for utilization in the indentation, and the results are shown in Fig. 5. With an increase in the loading force, the X- and Y-indentation widths as well as the indentation depth increase. It is noted here that all sizes shown in Fig. 5 are smaller than those of Fig. 3. This is because the wedge-shaped cantilever (see Fig. 2(d)) makes smaller indentation widths on the thinner polymer. In Fig. 5, the indentation depth is equal to the polymer thickness at 2.7 μN loading force and becomes larger than that at a loading force of >3.6 μN. Thus, 3.6 μN-indentation samples were employed in the following experiments.

Fig. 6(a) and (b) respectively show an AFM image of the 3.6-μN indentation sample and an SEM image of the same sample after the Pt electrodeposition was conducted at an electrode potential of 0.1 V vs RHE. In Fig. 6(a), nine indentation spots of 20 nm × 40 nm widths, which are smaller than those seen in Fig. 4, are obtained with an interdistance of 500 nm.

From Fig. 6(b), Pt electrodeposition is known to occur not only at the indentation spots but also on other sites outside the indentation. The thinner 10 ± 1-nm polymer seems to make it difficult to retain the insulation.

3.4. Optimization of electrode potential for Pt electrodeposition

In order to ensure that Pt deposition occurs only at the indentation spots on the 10 ± 1 nm polymer layer, an optimization of electrode potential for the electrodeposition will be needed. By changing the electrode potential between 0.1 and 0.3 V vs RHE, the Pt deposition was carried out for the same substrate as that shown in Fig. 6(a). First, the electrode potential was gradually changed from 0.30 to 0.10 V vs RHE. Pt depositon was not observed at 0.30, 0.20, and 0.15 V vs RHE; however, particulate deposition occurred at indentation spots and other sites at 0.10 V vs RHE. This means that the data reproduce the results of Fig. 6(b).

For the second substrate, the electrode potential was gradually shifted from 0.15 to 0.12 V vs RHE. As a result, Pt deposition did not occur at 0.15, 0.14, and 0.13 V vs RHE. After that, the Pt deposition occurred only at the indentation spots at 0.12 V vs RHE.

The third one was used for Pt electrodeposition at 0.12 V vs RHE, again, to ensure the results of the second substrate. Then, the Pt deposition certainly occurred. Fig. 7(a) and (b) respectively show an AFM image before the deposition and an SEM image after the deposition controlled at 0.12 V vs RHE. It is confirmed from the EDS analysis that the Pt deposition occurs only at the indentation spots. The deposited particle size is effectively reduced to 30–60 nm in diameter.

Consequently, the developed mask indentation technique for the thin 10 ± 1 nm polymer layer enables creating 20 nm × 40 nm width spots at an arbitrary distance. After electrodeposition at 0.12 V vs RHE, small 30–60 nm Pt particles were successfully deposited only at the indentation spots. The thus prepared Pt electrocatalyst of defined morphology can provide high effective

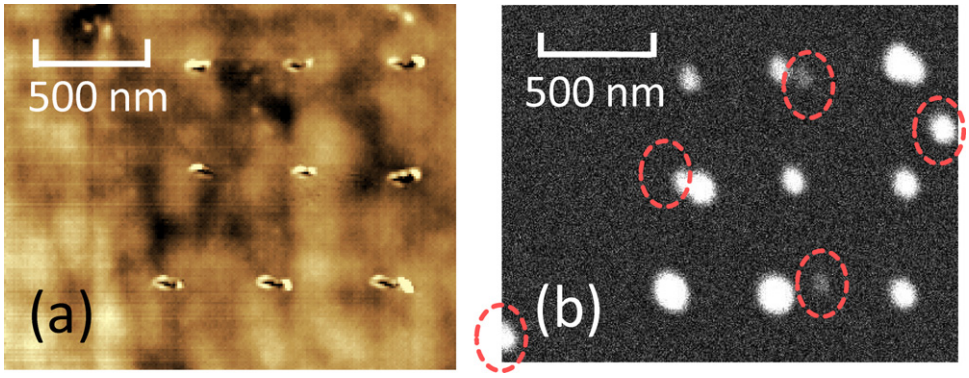

Fig. 6. (a) AFM image of a glassy carbon substrate coated with a 10 ± 1-nm polymer layer using the cantilever indentation at 3.6 μN loading force. (b) SEM image of the same sample after the Pt electrodeposition at 0.10 V vs RHE. Dashed circles indicate Pt deposition occurred outside the indentation area.

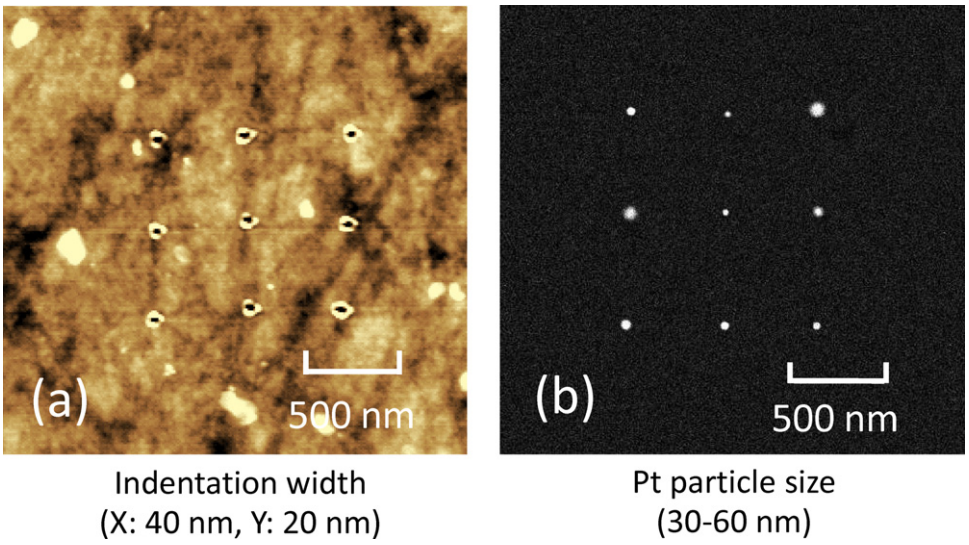

Fig. 7. A 10 ± 1-nm polymer-coated glassy carbon substrate indented by a cantilever at 3.6 μN loading force. (a) AFM image and (b) SEM image respectively show the same sample before and after the Pt electrodeposition at 0.12 V vs RHE.

surface area and regulate local microenvironments [4], which are preferably used for electrocatalytic-reaction-based electrochemical sensors, for instance, hydrogen gas [42], hydrogen peroxide[43], and formaldehyde [44] detectors.

4. Conclusions

To fabricate an electrocatalyst model, a mask indentation technique was newly developed to prepare small Pt particles on a glassy carbon electrode as follows:

(1) An electroconductive glassy carbon substrate was overcoated by a uniform insulating polymer layer of 10 ± 1 nm thick as a mask.
(2) A part of the polymer layer was removed by an indentation with the AFM cantilever. An optimized loading force of 3.6 μN formed the smallest exposed area of 20 nm × 40 nm.
(3) Pt electrodeposition was conducted at an electrode potential of 0.12 V vs RHE so that the Pt particle could be deposited only at the exposed deposition sites. Thus, Pt deposition of 30–60 nm in diameter was successfully formed.

Consequently, the Pt electrocatalyst of defined morphology in which the particle size and interparticle distance are independently controlled is fabricated.

Acknowledgement

This work was supported by a Grant-in-Aid for Scientific Research (B, 21360358) from the Japan Society for the Promotion of Science (JSPS), Japan.

References

[1] W. Vielstich, H. Yokokawa, H.A. Gasteiger, Handbook of Fuel Cells, Vol.5, Wiley, Singapore, 2009, Part 1.
[2] S. Siracusano, V. Baglio, A. Stassi, R. Ornelas, V. Antonucci, A.S. Aricò, Int. J. Hydrogen Energy 36 (2011) 7822.
[3] E. Katz, I. Willner, J. Wang, Electroanalysis 16 (2004) 19.
[4] C.M. Welch, R.G. Compton, Anal. Bioanal. Chem. 384 (2006) 601.
[5] Y. Pio, H. Kim, J. Nanosci. Nanotechnol. 9 (2009) 2215.
[6] H. Yano, J. Inukai, H. Uchida, M. Watanabe, P.K. Babu, T. Kobayashi, J.H. Chung, E. Oldfield, A. Wieckowski, Phys. Chem. Chem. Phys. 42 (2006) 4932.
[7] L.C. Ordóñez, P. Roqueroc, P.J. Sebastiana, J. Ramiírezc, Int. J. Hydrogen Energy 32 (2007) 3147.
[8] Y. Takasu, N. Ohashi, X.G. Zhang, Y. Murakami, H. Minagawa, K. Yahikozawa, Electrochim. Acta 4 (1996) 2595.
[9] A.A. Tseng, Nanofabrication: Fundamentals and Applications, World Scientific, Singapore, 2008.
[10] B. Bhushan, Springer Handbook of Nanotechnology, Springer, Germany, 2004.
[11] H. Zhang, R. Jin, C.A. Mirkin, Nano Lett. 4 (2004) 1493.
[12] B.W. Maynor, Y. Li, J. Liu, Langmuir 17 (2001) 2575.
[13] L.A. Porter Jr., H.C. Choi, J.M. Schmeltzer, A.E. Ribble, L.C.C. Elliott, J.M. Buriak, Nano Lett. 2 (2002) 1369.
[14] H.S. Shin, H.J. Yang, Y.M. Jung, S.B. Kim, Vib. Spectrosc. 29 (2002) 79.
[15] P.S. Hale, P. Kappen, N. Brack, W. Prissanaroon, P.J. Pigram, J. Liesegang, Appl. Surf. Sci. 252 (2006) 2217.
[16] Y. Zhang, S. Maupai, P. Schmuki, Surf. Sci. Lett. 551 (2004) L33.
[17] D. Fujita, K. Sagisaka, Sci. Technol. Adv. Mater. 9 (2008) 013003.
[18] J.P. Rabe, S. Buchholz, Appl. Phys. Lett. 58 (1991) 7.
[19] P. Mesquida, A. Stemmer, Microelectron. Eng. 61 (2002) 671.
[20] R.M. Nyffenegger, R.M. Penner, Chem. Rev. 97 (1997) 1195.
[21] N. Kubo, T. Homma, Y. Hondo, T. Osaka, Electrochim. Acta 51 (2005) 834.
[22] E. Balaur, T. Djenizian, R. Boukherroub, J.N. Chazalviel, F. Ozanam, P. Schmuki, Electrochem. Commun. 6 (2004) 153.
[23] C.G. Choi, C. Kee, H. Schift, Curr. Appl. Phys. 6S1 (2006) e8.
[24] H. Li, J.M. Biser, J.T. Perkins, S. Dutta, R.P. Vinci, H.M. Chan, J. Appl. Phys. 103 (2008) 024315.
[25] P. Schmuki, L.E. Erickson, Phys. Rev. Lett. 85 (2000) 2985.
[26] V. Parekh, E. Chunsheng, D. Smith, A. Ruiz, J.C. Wolfe, P. Ruchhoeft, E. Svedberg, S. Khizroev, D. Litvinov, Nanotechnology 17 (2006) 2079.
[27] K. Kordás, J. Remes, S. Leppävuori, L. Nánai, Appl. Surf. Sci. 178 (2001) 93.
[28] C. Scheck, P. Evans, R. Schad, Appl. Phys. Lett. 86 (2005) 133108.
[29] S.H. Kim, K.D. Lee, J.Y. Kim, M.K. Kwon, S.J. Park, Nanotechnology 18 (2007) 055306.
[30] H. Sugimura, O. Takai, N. Nakagiri, J. Electroanal. Chem. 473 (1999) 230.
[31] L.A. Porter Jr., A.E. Ribbe, J.M. Buriak, Nano Lett. 3 (2003) 1043.
[32] Y. Zhang, E. Balaur, P. Schmuki, Electrochim. Acta 51 (2006) 3674.
[33] H. El-Sayed, M.T. Greiner, P. Kruse, Appl. Surf. Sci. 253 (2007) 8962.
[34] L. Santinacci, T. Djenizian, H. Hildebrand, S. Ecoffey, H. Mokdad, T. Campanella, P. Schmuki, Electrochim. Acta 48 (2003) 3123.
[35] S.Y. Chou, P.R. Krauss, P. Renstrom, J. Appl. Phys. Lett. 67 (1995) 21.
[36] H.J.H. Chen, L.C. Chen, C. Lien, S.R. Chen, Y.L. Ho, Microelectron. Eng. 85 (2008) 1561.
[37] A.D. Taylor, B.D. Lucas, L.J. Guob, L.T. Thompsona, J. Power Sources 171 (2007) 218.
[38] J.H. Lee, K.Y. Yang, S.H. Hong, H. Lee, K.W. Choi, Microelectron. Eng. 85 (2008) 710.
[39] M. Fukuhara, J. Mizuno, M. Saito, T. Homma, S. Shoji, IEEJ Trans. Elect. Elect. Eng. 2 (2007) 307.
[40] A. Kishi, M. Umeda, Appl. Surf. Sci. 255 (2009) 9154.
[41] M. Umeda, Y. Kuwahara, A. Nakazawa, M. Inoue, J. Phys. Chem. C 113 (2009) 15707.
[42] D. Ding, Z. Chen, S. Rajaputra, V. Singh, Sens. Actuators B 124 (2007) 12.
[43] X.M. Miao, R. Yuan, Y.Q. Chai, Y.T. Shi, Y.Y. Yuan, J. Electroanal. Chem. 612 (2008) 157.
[44] Z.L. Zhou, T.F. Kang, Y. Zhang, S.Y. Cheng, Mikrochim. Acta 164 (2009) 133.